JOURNAL OF PROPULSION AND POWER
Vol. 15, No. 3, May–June 1999

Technical Notes

TECHNICAL NOTES are short manuscripts describing new developments or important results of a preliminary nature. These Notes cannot exceed 6 manuscript pages and 3 figures; a page of text may be substituted for a figure and vice versa. After informal review by the editors, they may be published within a few months of the date of receipt. Style requirements are the same as for regular contributions (see inside back cover).

Biharmonic Three-Dimensional Grid Generation for Axial Turbomachinery with Tip Clearance

G. A. Gerolymos* and G. Tsanga†
Universite Pierre-et-Marie-Curie,
91405 Orsay, Paris, France

Introduction

ALTHOUGH unstructured grids for turbomachinery computational fluid dynamics (CFD)[1] can handle geometries of arbitrary complexity, most turbomachinery blading can be adequately meshed using structured multiblock strategies,[2,3] which offer algorithmic simplicity and are well adapted to efficient implicit Navier–Stokes solvers.[3] Invariably, three-dimensional turbomachinery grids are obtained by stacking two-dimensional blade-to-blade grids,[2] which are generated using algebraic and/or elliptic procedures.[2] The basic elliptic procedure of Thompson et al.[4] imposes orthogonality on grid boundaries but does not control the distribution of the grid points on the boundaries. Steger and Sorenson[5] extended this technique by using Poisson equations with suitably adjusted source terms, allowing control of both grid spacing and orthogonality at the boundaries. Basson et al.[2] state that "the amount of control that can be obtained by the source terms is inadequate for cascade grids with thick leading- and trailing-edges." Another technique used in this paper, which has not yet been exploited for turbomachinery applications, is based on the solution of a biharmonic equation.[6,7] Because the biharmonic equation is a fourth-order partial differential equation, admitting combined Dirichlet and von Neumann boundary conditions, both positions and slopes are controlled at the boundaries, thus obtaining high-quality orthogonal grids (grid points on the pitchwise boundaries between channels coincide) in a quite straightforward way.

The computational domain is separated in three blocks, corresponding to a basic H−O−H grid.[3] The O block around the blade may contain subdomains to accurately resolve tip-clearance gaps. The N_k nodes in the radial direction (k wise) are stretched near the hub ($\frac{1}{3}N_k$) and near the casing ($\frac{1}{3}N_k$). The stretching is geometric with ratio r_k. The remaining $\frac{1}{3}N_k$ nodes are equally distributed in between. Using the nomenclature of the Appendix,

$$R(k) = R_{\text{HUB}} + l_{gs}(k,\, R_{\text{CASING}} - R_{\text{HUB}},\, N_k,\, \tfrac{1}{3}N_k,\, r_k,\, \tfrac{1}{3}N_k,\, r_k)$$

Finally, it is indispensable to correctly mesh the tip-clearance region, eventually present in rotors (at the casing) or in stators (at the hub).[2,3] Inside the tip-clearance gap, an O-type grid is used, also generated biharmonically. The tip-clearance grid is stretched both at the blade tip and at the casing (rotors), or the hub (stators).

Received April 17, 1998; revision received Sept. 17, 1998; accepted for publication Sept. 17, 1998. Copyright © 1999 by the American Institute of Aeronautics and Astronautics, Inc. All rights are reserved.

*Professor, Director, Laboratoire d'Energetique, Unite Associee au Centre National de Recherche Scientifique, Bâtiment 511.

†Graduate Student, Laboratoire d'Energetique, Unite Associee au Centre National de Recherche Scientifique, Bâtiment 511.

Blade-to-Blade Surface Grid

The blade-to-blade surface grid generation procedure is illustrated for a turbine cascade.[8] Let (x, R, θ) be a cylindrical coordinate's system, with $\boldsymbol{e}_x$ being the engine axis. On each $k = \text{const}$ surface (Fig. 1), a two-dimensional blade-to-blade plane is defined by the projection $[\hat{x} = x,\ \hat{y} = -R_{\text{LTE}}(k)\theta]$, where $R_{\text{LTE}}(k) = \frac{1}{2}[R_{\text{LE}}(k) + R_{\text{TE}}(k)]$ is a mean radius of the surface (average of leading- and trailing-edge radii). The leading edge (LE) and trailing edge (TE) on the blade (Fig. 1) are defined by prescribing the curvilinear distance from the $x_{\min}$ and $x_{\max}$ locations on the blade section. (This distance is given as a fraction of axial chord $\chi_x = x_{\max} - x_{\min}$: $s_{\text{LE}} = SP_{\text{LE}}\chi_x$ and $s_{\text{TE}} = SP_{\text{TE}}\chi_x$; it is positive toward the lower surface and negative toward the upper surface.) These points (LE and TE) separate the upper surface $(\cdot)_-$ and the lower surface $(\cdot)_+$: $\theta_-(x) \le \theta_+(x)\ \ \forall x \in (x_{\min}, x_{\max})$.

There is the same number $N_\pm$ of grid points on the upper $(-)$ and on the lower $(+)$ surface (corresponding to $N_i = 2N_\pm - 1$ points on the blade), stretched near the LE ($\frac{1}{3}N_\pm$ points with ratio $r_{i\text{LE}}$) and near the TE ($\frac{1}{3}N_\pm$ points with ratio $r_{i\text{LE}}$), with $\frac{1}{3}N_\pm$ points equidistant in curvilinear length in between (Fig. 1). The curvilinear coordinates are $s_\pm(n) = l_{gs}(n, L_\pm, N_\pm, \frac{1}{3}N_\pm, r_{i\text{LE}}, \frac{1}{3}N_\pm, r_{i\text{TE}})$, where l_{gs} is given in the Appendix, L_- is the curvilinear length of the upper surface, and L_+ is the curvilinear length of the lower surface [point LE corresponds to $s_\pm(1) = 0$].

There are N_i points on the outer ($j = N_j$) boundary, with N_u (N_d) points on the upstream (downstream) boundary, at an axial distance $\mathrm{d}x_u$ ($\mathrm{d}x_d$) from the $x_{\min}$ ($x_{\max}$) point (Fig. 1). The periodic part of the $j = N_j$ boundary is at middistance between adjacent blades for $x_{\min} + XP_{\text{LE}}\chi_x \le x \le x_{\min} + XP_{\text{TE}}\chi_x$, and extends upstream (downstream) by parabolas perpendicular to the upstream (downstream) boundary. The choice of XP_{LE} and XP_{TE} defines the θ position of the upstream and downstream parts of the $j = N_j$ boundary. The points on the periodic part of the $j = N_j$ boundary coincide between adjacent channels. They are distributed between the upstream boundary $i_{u1,2}$ (Fig. 1) and the downstream boundary $i_{d1,2}$, using geometric stretching ($\frac{1}{3}$ of the $i_{d_2} - i_{u_2} + 1 = i_{u_1} - i_{d_1} + 1$ points with ratio r_u upstream, and $\frac{1}{3}$ of the points with ratio r_d downstream).

The correspondence between the $j = N_j$ boundary points and the $j = 1$ boundary points is established by the choice of two corresponding points [$l_- \in (1, N_\pm)$ on the upper surface with $l_+ \in (1, N_\pm)$ on the lower surface, l being the point index from LE on each surface]. This choice greatly influences grid quality.

Biharmonic Solver

After defining the boundary points $(\hat{x}_B, \hat{y}_B)$, at $j = 1$ and at $j = N_j$ (Fig. 1), the blade-to-blade surface grid is generated biharmonically. The coordinates ξ and η along grid lines are defined in the interval [0, 1] [$\xi = (i-1)/(N_i - 1)$, $\eta = (j-1)/(N_j - 1)$]. The grid lines are the solution of the biharmonic equation in the $(\hat{x}, \hat{y})$ space $\mathfrak{D}_{2\text{D}}$ [with Laplacian operator $\nabla^2(\cdot) = \partial^2(\cdot)/\partial\hat{x}^2 + \partial^2(\cdot)/\partial\hat{y}^2$], with boundary conditions of position and orthogonality at the boundary $\partial\mathfrak{D}_{2\text{D}}$ of $\mathfrak{D}_{2\text{D}}$:

$$\begin{gathered}\nabla^4\xi = 0, \qquad \nabla^4\eta = 0 \quad \forall(\hat{x}, \hat{y})^T \in \mathfrak{D}_{2\text{D}} \\ (\hat{x}, \hat{y})^T = (\hat{x}_B, \hat{y}_B)^T \quad \forall(\hat{x}, \hat{y})^T \in \partial\mathfrak{D}_{2\text{D}}, \qquad \boldsymbol{e}_\eta \cdot \boldsymbol{n}_B = 0 \\ \xi = 0, 1, \qquad \boldsymbol{e}_\xi \cdot \boldsymbol{n}_B = 0, \qquad \eta = 0, 1\end{gathered} \tag{1}$$

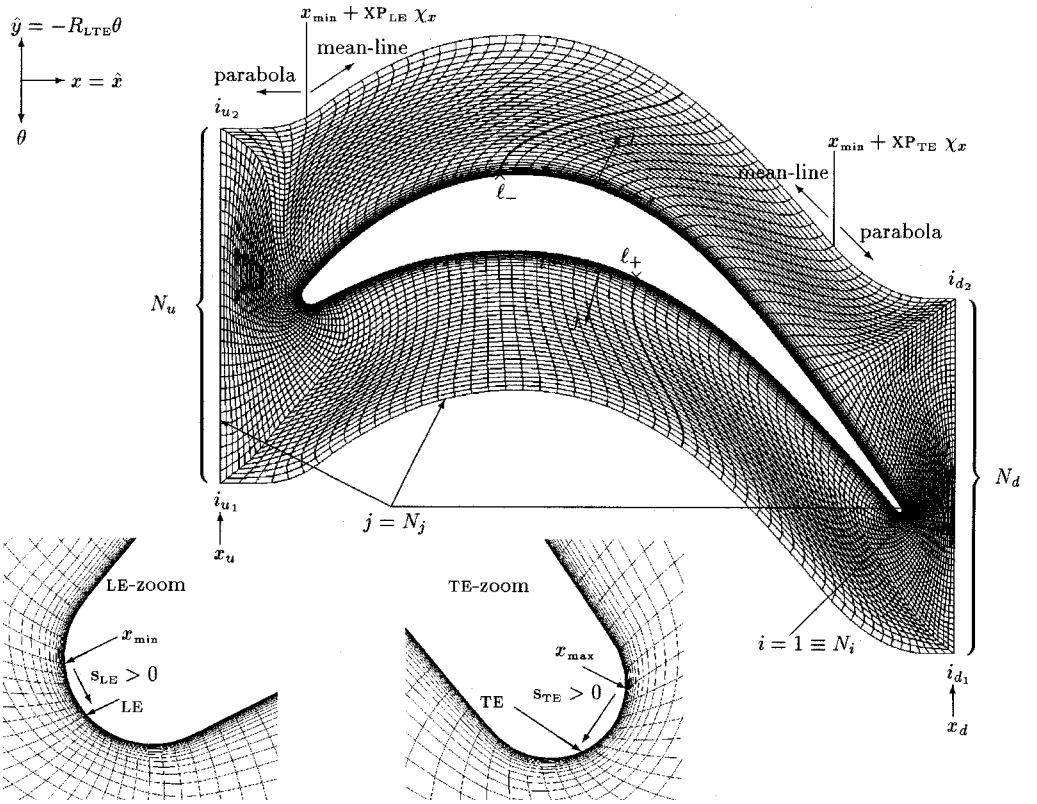

Fig. 1 Parameters for biharmonic blade-to-blade grid of a turbine cascade.[8]

where $\boldsymbol{n}_B$ is the unit normal on the boundary, and $\boldsymbol{e}_\xi$ ($\boldsymbol{e}_\eta$) the unit vector ξ wise (η wise). It is simpler[7] to solve this fourth-order problem [Eq. (1)] as two coupled second-order problems,

$$\nabla^2\xi = Q_\xi, \qquad \nabla^2 Q_\xi = 0, \qquad \nabla^2\eta = Q_\eta$$
$$\nabla^2 Q_\eta = 0 \quad \forall[\hat{x}, \hat{y}]^T \in \mathcal{D}_{2D} \tag{2}$$

with boundary conditions

$$(\hat{x}, \hat{y})^T = (\hat{x}_B, \hat{y}_B)^T \quad \forall(\hat{x}, \hat{y})^T \in \partial\mathcal{D}_{2D}$$
$$Q_\eta = \nabla^2\eta - 10^{n_0}\frac{\partial\eta}{\partial n_B}, \qquad \xi = 0, 1 \tag{3}$$
$$Q_\xi = \nabla^2\xi - 10^{n_0}\frac{\partial\xi}{\partial n_B}, \qquad \eta = 0, 1$$

This is equivalent, as clearly stated by Sparis,[6] "to iteratively adjusting the source term in the Poisson equation to control simultaneously the mesh density and the skewness at the boundary surfaces." The orthogonality boundary conditions are now applied numerically using an adjustable constant 10^{n_0} (for turbomachinery applications $n_0 = 3$–7 with $\hat{x}$ and $\hat{y}$ in meters).[7]

The resulting system of equations can be inverted to use ξ and η as independent variables by using the inverted Laplacian operator[4]:

$$\mathcal{D}(\cdot) = \left[\left(\frac{\partial\hat{x}}{\partial\eta}\right)^2 + \left(\frac{\partial\hat{y}}{\partial\eta}\right)^2\right]\frac{\partial^2(\cdot)}{\partial\xi^2} - 2\left(\frac{\partial\hat{x}}{\partial\xi}\frac{\partial\hat{x}}{\partial\eta} + \frac{\partial\hat{y}}{\partial\xi}\frac{\partial\hat{y}}{\partial\eta}\right)\frac{\partial^2(\cdot)}{\partial\xi\partial\eta}$$
$$+\left[\left(\frac{\partial\hat{x}}{\partial\xi}\right)^2 + \left(\frac{\partial\hat{y}}{\partial\xi}\right)^2\right]\frac{\partial^2(\cdot)}{\partial\eta^2} \tag{4}$$

The resulting system [with boundary conditions given by Eqs. (3)] is[7]

$$\mathcal{D}\left(\begin{bmatrix}\hat{x}\\ \hat{y}\\ Q_\xi\\ Q_\eta\end{bmatrix}\right) = -J^2\begin{bmatrix}Q_\xi\dfrac{\partial\hat{x}}{\partial\xi} + Q_\eta\dfrac{\partial\hat{x}}{\partial\eta}\\ Q_\xi\dfrac{\partial\hat{y}}{\partial\xi} + Q_\eta\dfrac{\partial\hat{y}}{\partial\eta}\\ 0\\ 0\end{bmatrix} \tag{5}$$

$$J = \frac{\partial\hat{x}}{\partial\xi}\frac{\partial\hat{y}}{\partial\eta} - \frac{\partial\hat{y}}{\partial\xi}\frac{\partial\hat{x}}{\partial\eta}, \qquad \forall\xi \in]0, 1[; \quad \forall\eta \in]0, 1[$$

$$Q_\xi = \nabla^2\xi = \frac{1}{J}\left[\frac{\partial\hat{y}}{\partial\eta}\mathcal{D}(\hat{x}) - \frac{\partial\hat{x}}{\partial\eta}\mathcal{D}(\hat{y})\right]$$
$$Q_\eta = \nabla^2\eta = -\frac{1}{J}\left[\frac{\partial\hat{y}}{\partial\xi}\mathcal{D}(\hat{x}) - \frac{\partial\hat{x}}{\partial\xi}\mathcal{D}(\hat{y})\right] \tag{6}$$
$$\forall\xi \in]0, 1[; \quad \forall\eta \in]0, 1[$$

and is solved iteratively by successive underrelaxation (with factor $\frac{1}{2}$; for turbomachinery applications 500–1000 iterations are needed).

The blade-to-blade O grid (Fig. 1) contains four corners at the $j = N_j$ boundary (points i_{d_1}, i_{u_1}, i_{u_2}, i_{d_2}), where the normal to the boundary $\boldsymbol{n}_B$ is not uniquely defined. The orthogonality condition is not applied in the neighborhood of these points ($|i - i_{d_1}|$, $|i - i_{u_1}|$, $|i - i_{u_2}|$, $|i - i_{d_2}| = 0, 1, 2, 3, 4$). The $i = 1, N_i$ boundary points are treated as internal points exploiting O-grid periodicity.

After the end of the biharmonic solver iterations, the grid points are stretched geometrically j wise along $i = \text{const}$ lines

($\frac{1}{2}N_j$ points near the blade with ratio r_j, and the remaining $\frac{1}{2}N_j$ points are equidistant). Using the nomenclature of the Appendix, the curvilinear coordinate along an $i = \text{const}$ line of length L is $s(j) = l_{gs}(j; L, N_j, \frac{1}{2}N_j, r_j, 1, 1)$. Stretching is done by piecewise quintic interpolation of i-wise curvilinear coordinates on the initial biharmonic grid. This corresponds to redefining the $j = \text{const}$ lines, and preserves orthogonality.

Tip-Clearance Grid

The $N_{k_{TC}}$ points in the radial direction within the gap (Fig. 2) are stretched at the casing ($\frac{1}{2}N_{k_{TC}}$) and at the blade tip ($\frac{1}{2}N_{k_{TC}}$), with ratio $r_{k_{TC}}[R_{TC}(k_{TC}) = R_{TIP} + l_{gs}(k_{TC}; R_{CASING} - R_{TIP}, N_{k_{TC}}, \frac{1}{2}N_{k_{TC}}, r_{k_{TC}}, \frac{1}{2}N_{k_{TC}}, r_{k_{TC}})$, with l_{gs} defined in the Appendix]. On each radial surface, the tip-clearance (TC) gap is discretized using a biharmonically generated O-type grid, whose innermost line ($j_{TC} = 1$) collapses into a curve, lying on the profile camberline. The camberline passes from the LE and TE points (Fig. 1), and is defined approximately as a pointwise average between the upper and lower surface $\{x_C(n) = \frac{1}{2}[x_-(n) + x_+(n)];\ \theta_C(n) = \frac{1}{2}[\theta_-(n) + \theta_+(n)];\ n = 1, \ldots, N_\pm\}$. The TC grid (Fig. 2) has singular triple points, STP_{LE} at the leading edge ($i_{LE} - 1$, i_{LE}, $i_{LE} + 1$ at $j_{TC} = 1$) and STP_{TE} at the trailing edge ($i_{TE} - 1$, i_{TE}, $i_{TE} + 1$ at $j_{TC} = 1$). Point $STP_{LE} = (i_{LE}, 1)$ is on the camberline at a curvilinear distance from point $LE = (i_{LE}, N_{j_{TC}})$ equal to the average curvilinear distance on the blade surface between point LE and its neighbors $(i_{LE} \pm 1, N_{j_{TC}})$ (Fig. 2). Denoting s_C as the curvilinear coordinate along the camberline [$s_C(LE) = 0$] and $s_\pm$ as the curvilinear coordinates along the upper ($-$) and lower ($+$) surfaces [$s_\pm(LE) = 0$],

$$s_C(STP_{LE}) = \tfrac{1}{2}\left[s_-\left(i_{LE} + 1, N_{j_{TC}}\right) + s_+\left(i_{LE} - 1, N_{j_{TC}}\right)\right]$$

$$L_C - s_C(STP_{TE}) = \tfrac{1}{2}\left[L_- - s_-\left(i_{TE} - 1, N_{j_{TC}}\right) + L_+ - s_+\left(i_{TE} + 1, N_{j_{TC}}\right)\right] \tag{7}$$

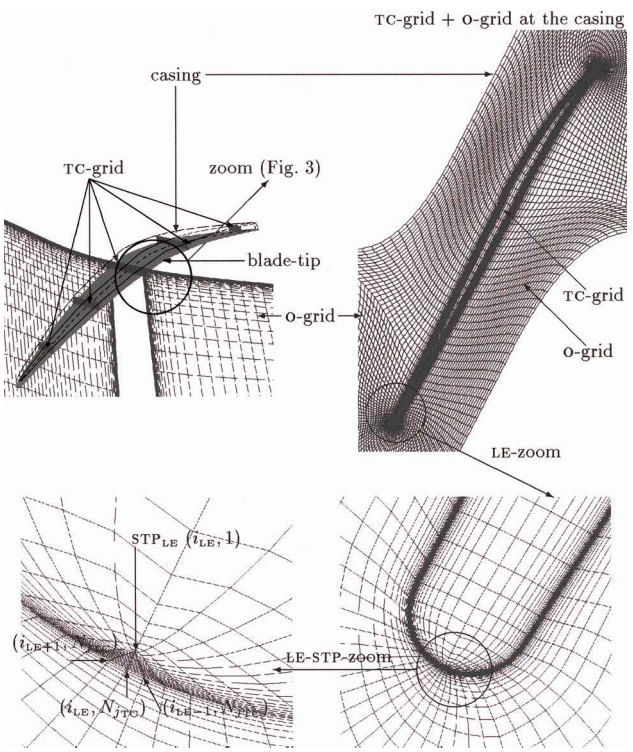

Fig. 2 Typical tip-clearance grid of a transonic compressor rotor.

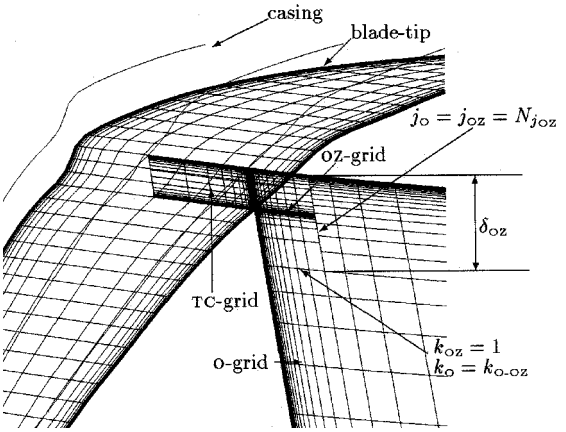

Fig. 3 Detail from Fig. 2, showing the matching of the tip-clearance (TC) grid with the external grid (O) of a transonic compressor rotor,[3] using a patched grid (OZ).

where L_C, L_-, and L_+ are the curvilinear lengths of the camberline, the upper surface, and the lower surface, respectively. The points on the $j_{TC} = 1$ line (portion of the camberline joining the two singular points) are stretched near the singular points in the same way as the points on the blade surface are stretched at the leading and trailing edge. The i-wise distribution of points on the outer boundary (blade surface) is the one used for the blade O grid. After the biharmonic generation of the tip-clearance grid, the $N_{j_{TC}}$ points from the blade camberline to the external O grid are geometrically stretched, with j-wise grid-size matching at the TC–O boundary (there are $2N_{j_{TC}}$ points across the blade within the gap).

The $i_{TC} = \text{const}$ surfaces of the TC grid coincide with the $i_O = \text{const}$ surfaces of the O grid ($N_{i_{TC}} \equiv N_{i_O}$), but the two grids have different radial (k-wise) distributions (Fig. 3), because the TC grid is stretched both at the casing and at the blade tip, whereas the O grid is stretched only at the casing. This original technique was introduced to render the blade O grid independent of the exact position of the blade tip,[3] and to apply grid clustering at the blade tip only in the neighborhood of the blade (Fig. 3).

The tip-clearance flow that leaves the blade tip forms a jetlike structure that interacts with the interblade flowfield.[9] To capture this structure correctly, a patched O-zoom (OZ) grid was introduced (Fig. 3). This OZ grid spans radially from the casing to a given radial depth δ_{OZ} beneath it. The $i_{OZ} = \text{const}$ surfaces and the $j_{OZ} = \text{const}$ surfaces of the OZ grid coincide with the $i_O = \text{const}$ and the $j_O = \text{const}$ surfaces of the O grid. In the radial direction, the OZ-grid points coincide with the TC-grid points at the TC–OZ boundary. Denoting $R_{TC}(k_{TC})$ as the $N_{k_{TC}}$ radial surfaces of the TC grid and $R_{OZ}(k_{OZ})$ as the $N_{k_{OZ}}$ radial surfaces of the OZ grid,

$$R_{OZ}(k_{OZ}) = R_{TC}\left(k_{TC} = k_{OZ} + N_{k_{TC}} - N_{k_{OZ}}\right)$$
$$k_{OZ} = N_{k_{OZ}} - N_{k_{TC}} + 1, \ldots, N_{k_{OZ}} \tag{8}$$

The OZ-grid points are stretched beneath the blade tip until an O-grid radial surface $k_O = k_{O-OZ}$, where the OZ-grid points coincide with the O-grid points. Denoting $R_O(k_O)$ as the N_{k_O} radial surfaces of the O grid,

$$R_{OZ}(k_{OZ}) = R_{TIP} - [R_{TC}(2) - R_{TC}(1)]\frac{r_{OZ}^{\left(N_{k_{OZ}} - N_{k_{TC}} - k_{OZ}\right)} - 1}{r_{OZ} - 1}$$
$$k_{OZ} = 1, \ldots, N_{k_{OZ}} - N_{k_{TC}} \tag{9}$$

where r_{OZ} is computed to give the correct distance $R_{TIP} - R_O(k_{O-OZ})$.

Conclusions

In the present work, a methodology for three-dimensional structured multiblock grid generation in axial turbomachinery was presented. There is a main O grid around each blade, constructed by stacking two-dimensional blade-to-blade surface O grids generated biharmonically. Only a few user-defined parameters are needed for generating the blade-to-blade surface O grids, and experience has shown that the choice of these parameters is a quite straightforward task. Biharmonic grid generation ($\nabla^4\xi=0$, $\nabla^4\eta=0$) has the decisive advantage over elliptic grid generation ($\nabla^2\xi=Q_\xi$, $\nabla^2\eta=Q_\eta$) in that it allows automatic control of both position and orthogonality at the boundaries. The numerical implementation used ($\nabla^2\xi=Q_\xi$, $\nabla^2 Q_\xi=0$; $\nabla^2\eta=Q_\eta$, $\nabla^2 Q_\eta=0$) clearly shows that biharmonic grid generation computes the source terms Q_ξ and Q_η, which are user-defined in Poisson grid generation. The biharmonic solver gives a quasiorthogonal initial grid that is not yet refined near the solid walls. Stretching to accurately resolve boundary layers is obtained by interpolating points on computed grid lines.

Tip-clearance gaps are meshed using O-type grids, generated biharmonically. The radial surfaces of the main blade-to-blade surface O grid are stretched near the casing and the hub. The clearance-gap TC grid is stretched both at the casing and at the blade tip. The radial distribution of the TC grid is independent of the radial distribution of the O grid. A buffer OZ grid that overlaps with the O grid, and that is stretched both at the casing and at the blade tip, is used to accurately resolve the flow coming over the tip.

The method is quite robust and provides good-quality structured grids. It has been applied to the computation of various compressor and turbine configurations using a three-dimensional Navier–Stokes solver with multiequation turbulence closures.[3,9] In the case of stators with clearance gap at the hub, grid generation is done in an exactly analogous way.

Appendix: Geometric Stretching

The geometric stretching used stretches N_1 of the N points near the starting location [$s_1=s(1)=0$] with ratio r_1, stretches N_2 points near the final location [$s_2=s(N)=L$] with ratio r_2, and places $N-N_1-N_2$ equidistant points in between:

$$l_{gs}(n, L, N, N_1, r_1, N_2, r_2)=\begin{cases} s(1)+\dfrac{r_1^{n-1}-1}{r_1-1}hr_1^{-(N_1-2)}, & n=2,\ldots,N_1 \\ s(N_1)+(n-N_1)h, & n=N_1+1,\ldots,N-N_2+1 \\ s(N-N_2+1)+\dfrac{r_2^{-(n-N+N_2-1)}-1}{r_2^{-1}-1}h, & n=N-N_2+2,\ldots,N \end{cases} \tag{A1}$$

$$h=L\left[N-N_1-N_2+1+\frac{r_1^{-(N_1-1)}-1}{r_1^{-1}-1}+\frac{r_2^{-(N_2-1)}-1}{r_2^{-1}-1}\right]^{-1} \tag{A2}$$

References

[1]Dawes, W. N., "The Simulation of 3-D Viscous Flow in Turbomachinery Geometries Using a Solution-Adaptive Unstructured Mesh Methodology," *Journal of Turbomachinery*, Vol. 114, July 1992, pp. 528–537.

[2]Basson, A. H., Kunz, R. F., and Lakshminarayana, B., "Grid Generation for 3-D Turbomachinery Geometries Including Tip Clearance," *Journal of Propulsion and Power*, Vol. 9, No. 1, 1993, pp. 59–66.

[3]Gerolymos, G. A., Tsanga, G., and Vallet, I., "Near-Wall k-ϵ Computation of Transonic Turbomachinery Flows with Tip-Clearance," *AIAA Journal*, Vol. 36, No. 10, 1998, pp. 1769–1777.

[4]Thompson, J. F., Thames, F. C., and Mastin, C. W., "Automatic Numerical Generation of Body-Fitted Curvilinear Coordinate System for Field Containing any Number of Arbitrary 2-D Bodies," *Journal of Computational Physics*, Vol. 15, 1974, pp. 299–319.

[5]Steger, J. L., and Sorenson, R. L., "Automatic Mesh-Point Clustering near a Boundary in Grid Generation with Elliptic Partial Differential Equations," *Journal of Computational Physics*, Vol. 33, 1979, pp. 405–410.

[6]Sparis, P. D., "A Method for Generating Boundary-Orthogonal Curvilinear Coordinate Systems Using the Biharmonic Equation," *Journal of Computational Physics*, Vol. 61, 1985, pp. 445–462.

[7]Sparis, P. D., and Karkanis, A., "Boundary-Orthogonal Biharmonic Grids via Preconditioned Gradient Methods," *AIAA Journal*, Vol. 30, No. 3, 1992, pp. 671–678.

[8]Fottner, L. (ed.), "Test Cases for Computation of Internal Flows in Aero Engine Components," AGARD Advisory Rept. 275, 1990, pp. 124–138.

[9]Gerolymos, G. A., and Vallet, I., "Tip-Clearance and Secondary Flows in a Transonic Compressor Rotor," *Journal of Turbomachinery* (to be published).

Adaptive Analysis of Oscillating Cascade Flows on a Quadrilateral–Triangular Mesh

S. Y. Yang*

National Huwei Institute of Technology, Yunlin 632, Taiwan, Republic of China

Introduction

In recent years, a number of Euler[1,2] and Navier–Stokes[3,4] solvers have been presented to simulate the blade vibration problems. Wolff and Fleeter[1] applied the Fourier series lagged boundary condition treatment on an expanded grid along the periodic boundary. Hwang and Yang[2] presented a rigid-deformable dynamic mesh algorithm to investigate transonic flows around an oscillating cascade of four blades. On a multipassage computational mesh,[3] the explicit four-stage Runge–Kutta scheme and the Baldwin–Lomax mixing-length turbulence model were adopted. The calculation showed that there was a more apparent mesh dependence of the results in the regions of flow separation. Within a composite grid where a deforming C-grid was embedded in an H-grid, a coupled inviscid/viscous model[4] was implemented to incorporate the inverse integral boundary-layer solution and the time-marching NPHASE analysis. The purpose of this work is to present a solution-adaptive solver to investigate the transonic oscillating cascade flows on a quadrilateral–triangular mesh. The Euler equations with moving domain effects are solved in the Cartesian coordinate. This solver

Received June 1, 1998; presented as Paper 98-3436 at the AIAA/ASME/SAE/ASEE 34th Joint Propulsion Conference, Cleveland, OH, July 13–15, 1998; revision received Dec. 3, 1998; accepted for publication Dec. 4, 1998. Copyright © 1999 by the American Institute of Aeronautics and Astronautics, Inc. All rights reserved.

*Associate Professor, Department of Aeronautical Engineering. Member AIAA.